International Conference on Science, Engineering & Management Trends

International Journal of Science, Engineering and Technology
ISSN: 2348-4098, P-ISSN: 2395-4752

Design and Finite Element Analysis of Disc Brake Wear at the Pad–Disc Interface Using Archard's Wear Law

Shivani Baban Suryawanshi[1] Prof. Dr. T.Y badgujar[2]
Department of Mechanical Engineering
Savitribai Phule Pune University, Pune

Abstract— Wear of the brake pad and rotor governs the durability, maintenance interval and reliability of passenger-car disc brakes. This paper presents a three-dimensional finite element (FE) framework for predicting wear at the pad–disc interface using a generalised form of Archard's wear law integrated with an explicit Euler scheme. A front brake corner is decomposed using modular system modelling and reduced to a piston–back plate–friction lining–rotor subsystem, which is analysed in ANSYS with frictional surface-to-surface contact. Wear is updated iteratively over 2900 rotor revolutions (≈2500 m of sliding). Static normal loading (2.5 kN) produces a symmetric pressure peak of about 1.2 MPa beneath the piston rim, whereas tangential friction (μ = 0.45) shifts the pressure to the leading edge and causes trailing-edge separation; running-in then progressively levels the pressure field. Three lining materials—organic, semi-metallic and ceramic-matrix composite—are compared. Maximum wear depth falls from 15.0 μm to 6.2 μm and 2.1 μm, while running-in lengthens from 2400 to 4100 and 5800 revolutions and the initial peak pressure rises from 1.20 to 2.10 MPa, exposing a stiffness–wear trade-off. The framework offers a basis for experimental validation and pad design optimisation.

Index Terms—Disc brake, brake pad wear, finite element analysis, Archard's wear law, contact pressure, friction materials

I. INTRODUCTION

The disc brake is a safety-critical subsystem of every modern passenger car. During braking, hydraulic pressure forces friction pads against a rotating rotor and the vehicle's kinetic energy is dissipated as heat through dry sliding friction. The same sliding contact removes material from the pad and rotor, a process known as wear. Wear changes surface geometry and the contact-pressure distribution, and so affects braking efficiency, noise, service life and maintenance cost.

Brake wear is a tribological problem. The friction coefficient sets the tangential force and heat generation, whereas contact pressure and sliding distance control the amount of material removed. Contact pressure is rarely uniform: pad geometry, stiffness, mounting and deformation create localised high-pressure zones that experience faster wear and greater frictional heating. These zones also change as the surfaces wear, so the pressure field and the wear depth evolve together during the running-in period of a new pad. Predicting this evolution is therefore central to understanding the durability of a brake.

International Journal of Science, Engineering and Technology
ISSN: 2348-4098, P-ISSN: 2395-4752

Physical wear testing on dynamometers is expensive and time-consuming, and it is hard to measure the local distribution of wear over the whole friction surface. Finite element analysis (FEA) offers a complementary route: the contact problem is solved numerically and the pressure field is fed into a wear law. The wear law most widely used is that of Archard [1], which relates the volume of removed material to normal load, sliding distance and hardness. Söderberg and Andersson [2] showed that Archard's law can be coupled with general-purpose FE software to simulate progressive pad wear and the resulting redistribution of contact pressure.

Despite this progress, predicted wear remains sensitive to geometry, contact modelling, wear coefficients and validation data, so a traceable procedure is needed for each brake assembly. This paper therefore: (i) develops a modular 3-D FE model of a passenger-car brake pad–rotor subsystem; (ii) implements an iterative Archard-based wear routine using explicit Euler integration; (iii) examines how tangential friction and running-in shape the pressure field; and (iv) compares organic, semi-metallic and ceramic-matrix linings in terms of pressure concentration, wear depth and running-in duration.



Fig. 1. Components of a passenger-car disc brake: caliper, hydraulic piston, brake pads, carrier and ventilated rotor.

II. LITERATURE REVIEW

1. Wear Prediction by Finite Element Analysis

Voloacă et al. [3] reviewed brake-pad wear and stressed that friction, pressure, sliding distance, temperature and material composition all influence material removal, so a single simplified relation may not suffice. Tang et al. [4] combined Archard's model with Abaqus, verified it with pin-on-disc tests and applied it to single- and three-piston brakes in a coupled wear–thermal–structural study. Gurumoorthy et al. [5] predicted pad wear and service life with a Rhee-type formulation and compared the results with laboratory and inertia-dynamometer data. Riva et al. [6] fed experimentally measured wear and emission maps into an FE model and obtained wear and particle emissions consistent with dynamometer measurements, while the friction map of [7] showed that the friction coefficient varies locally with pressure and velocity. Sha et al. [8] linked elastoplastic contact of rough surfaces with Archard theory to estimate disc wear and life, and Zhang et al. [9] used a DEFORM model to compute wear depth and volume in high-power braking. Han et al. [10] related uneven pad wear to non-uniform pressure and used shape optimisation to improve uniformity.

2. Contact Pressure and Thermal Effects

Abu Bakar and Ouyang [11] demonstrated that contact-pressure prediction depends strongly on geometry, mesh and contact definition, and that a uniform pressure assumption is not realistic. Ouyang et al. [12] used the calculated pressure to determine frictional heat flux and transient vibration, and Stoica et al. [13] showed that pad and disc compliance govern the pressure at the inner, middle and outer pad edges. Goo [14] inferred pressure distribution from infrared thermography. Material choice was addressed by Grześ et al. [15], who compared six pad materials against cast iron using temperature-

International Journal of Science, Engineering and Technology
ISSN: 2348-4098, P-ISSN: 2395-4752

dependent friction and wear, and by Olshevskiy et al. [16] and Cho and Cho [17], who emphasised coupled thermal–structural–wear behaviour and thermal deformation.

Table III summarises representative studies and their relevance to the present work.

Table III Summary Of Representative Related Studies

Ref.	Method	Relevance to this work
[4]	Archard + FEA, pin-on-disc verification	Wear routine; need for validation
[5]	FE wear with dynamometer comparison	Pad life prediction
[6]	FEA with wear and emission maps	Local pressure–velocity dependence
[8]	Elastoplastic contact + Archard	Roughness effect on wear
[10]	Thermo-mechanical FEA + shape optimisation	Pressure non-uniformity and uneven wear
[11]	3-D FE contact-pressure prediction	Contact modelling and mesh effects
[15]	FE thermal–wear material selection	Multi-criteria material choice

3. Research Gap

The reviewed studies establish that FE contact analysis and Archard-type laws can predict brake wear, but results depend on geometry, material data and validation. Few studies present, for one passenger-car subsystem, a complete chain from modular CAD decomposition and contact analysis through iterative wear updating to a like-for-like comparison of several friction materials. This paper addresses that chain.

III. METHODOLOGY

1. Modular System Model and CAD Geometry

A front brake corner comprises the knuckle, wheel bearing, floating single-piston caliper, ventilated rotor and two pads. Following the modular system modelling (MSM) approach used in [2], components are described by mating features and joined through interface models, so that only a reduced subsystem—hydraulic piston, piston-side pad and rotor—needs to be solved. A 3-D CAD model was built in Siemens Solid Edge with four bodies: piston, steel back plate, friction-material lining and ventilated cast-iron rotor (Fig. 2). Functional mating surfaces include the piston–plate contact, the plate–lining bonded face, the active lining–rotor sliding face and the rotor–hub joint.



Fig. 2. Simplified CAD assembly of the brake pad–rotor subsystem showing piston, back plate, friction material and rotor.

The mating surfaces are classified by function (Fig. 3). The piston has a contact face with the back plate, a rear face that receives hydraulic pressure and a cylindrical guide face. The back plate has a piston interface, a bonded interface with the lining and lateral abutment slots that slide against the caliper carrier. The lining has a bonded face and an active friction face, and the rotor has an active sliding

International Journal of Science, Engineering and Technology
ISSN: 2348-4098, P-ISSN: 2395-4752

surface and a hub mounting joint. Interfaces between these features are represented by explicit interface models, and the boundary conditions follow from the interaction matrix shown schematically in Fig. 4.

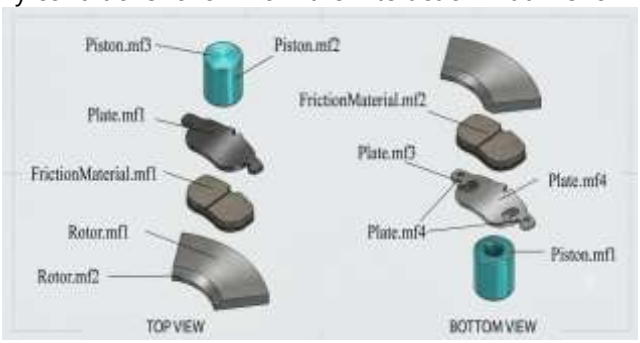


Fig. 3. Exploded CAD view showing the mating-feature interfaces of the piston, back plate, friction material and rotor.

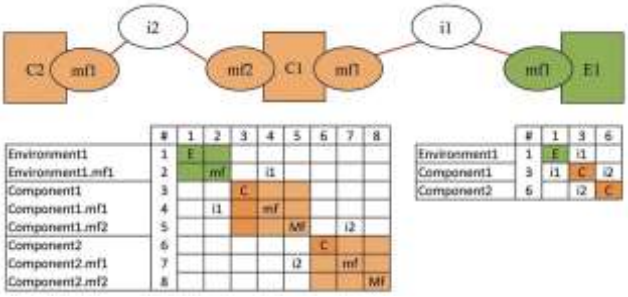


Fig. 4. Schematic of the modular subsystem: components, mating features (mf) and interface models (i) with their interaction matrix.

2. Finite Element Model and Boundary Conditions

The 3-D model was created in ANSYS v11.0. The back plate and friction lining are deformable and meshed with 8-node linear solid elements (SOLID185) of 3 mm characteristic size. The piston and rotor are rigid surfaces (TARGE170) tied to pilot nodes at their centre of mass and centre of rotation. The pad–rotor interface uses asymmetric surface-to-surface frictional contact (CONTA173/TARGE170) with an augmented Lagrangian algorithm in the normal and tangential directions. The plate–lining interface is bonded, and the piston–plate interface is frictionless sliding contact that permits separation (Fig. 5).

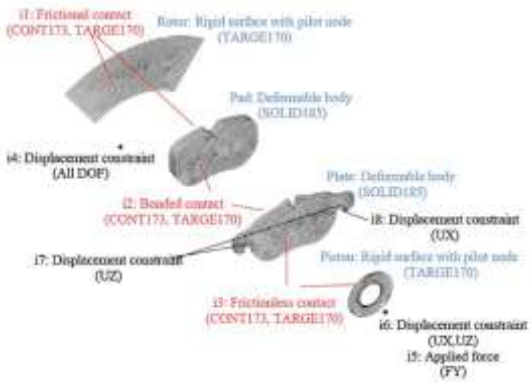


Fig. 5. FE model: element types, contact pairs (i1–i3) and boundary constraints (i4–i8).

A 3 mm element size was used over the lining so that the pressure gradients near the piston rim and the leading and trailing edges are resolved. Because the pad is deformable and the rotor is rigid, wear is evaluated on the friction lining; rotor wear is not considered in this model. The contact algorithm allows compressive pressure only and prevents interpenetration, and contact status is checked after each solution to confirm that separated regions (such as the trailing edge) are identified correctly.

International Journal of Science, Engineering and Technology
ISSN: 2348-4098, P-ISSN: 2395-4752

The piston pilot node is constrained in all translations except the axial direction, where a 2.5 kN force, equivalent to 1 MPa hydraulic line pressure, is applied. Rotor motion is imposed through the rotor pilot node (Fig. 6). Under a Coulomb assumption the tangential force is

$$Ff = \mu FN \quad (1)$$

where FN is the normal contact force and μ the friction coefficient.

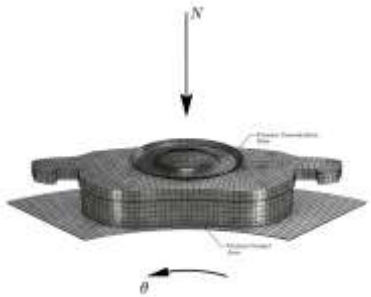


Fig. 6. FE loading conditions: normal force N on the piston and rotor rotation θ.

3. Wear Formulation

Archard's law states that the removed volume is

$$V = K FN s / H \quad (2)$$

where K is the wear coefficient, s the sliding distance and H the hardness of the wearing material. In local form, the wear depth is h = K p s/H, with p the local contact pressure. For the macroscopic pad model, the rate of wear depth with sliding distance is written with a dimensional coefficient k (Pa−1):

$$dh / ds = k p \quad (3)$$

For a surface node i at radius ri, nj rotor revolutions in step j give the sliding increment

$$\Delta si,j = nj \cdot 2\pi ri \quad (4)$$

and explicit Euler integration updates the cumulative nodal wear depth:

$$hi,j = hi,j-1 + k\, pi,j\, \Delta si,j \quad (5)$$

4. Iterative Wear Simulation

The routine is automated in ANSYS using APDL loops. Each iteration (1) generates or updates the FE model; (2) solves the static structural contact problem; (3) reads the nodal contact pressures; (4) computes nodal wear increments from (4) and (5); (5) moves the lining surface nodes inward and repositions the rigid boundaries to close contact gaps; and (6) stores the results and repeats until the prescribed revolutions are reached. Results are post-processed in MATLAB. Because the geometry is updated every step, the pressure field evolves as the pad wears in. The loop is summarised in Fig. 7.

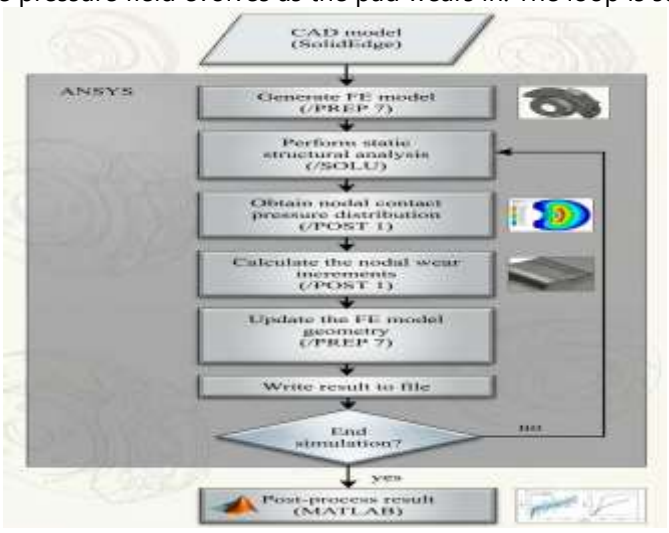


Fig. 7. Flowchart of the iterative FE wear simulation: model generation, static contact solution, nodal pressure extraction, wear increment calculation and geometry update, repeated until the end of the simulation.

International Journal of Science, Engineering and Technology
ISSN: 2348-4098, P-ISSN: 2395-4752

5. Modelling Assumptions

The following assumptions apply to the results presented:

- the analysis is isothermal; frictional heating and thermal expansion are not modelled;
- the piston and rotor are rigid, and the caliper is not represented explicitly;
- the wear coefficient k and friction coefficient μ are constant for each material;
- wear follows a linear Archard relation between wear depth, pressure and sliding distance; and
- the sliding distance is obtained from the prescribed rotor revolutions, with the sliding increment at each node proportional to its radius.

6. Friction Materials

Three lining candidates were evaluated against the organic baseline (Table I). Only the lining properties were changed; geometry, load, sliding distance and contact settings were kept constant so that differences arise from material behaviour alone.

Table I Friction-Lining Material Properties

Material	E (GPa)	ν	k (Pa^{-1})	μ
Organic composite (baseline)	10.0	0.10	1.0×10^{-14}	0.45
Semi-metallic lining	22.0	0.22	0.45×10^{-14}	0.38
Ceramic-matrix composite	35.0	0.18	0.15×10^{-14}	0.42

IV. RESULTS AND DISCUSSION

1. Effect of Tangential Friction on Contact Pressure

With a pure normal load of 2.5 kN and no rotor rotation, the contact pressure is symmetric and concentrated beneath the circular piston rim, with a peak of about 1.2 MPa; the outer edges of the pad carry no load. When rotation is prescribed with μ = 0.45, tangential traction produces a tipping moment on the pad. Pressure then concentrates strongly along the leading edge while the trailing edge separates (Fig. 8). A purely normal model therefore under-represents the localised loading that drives uneven wear.

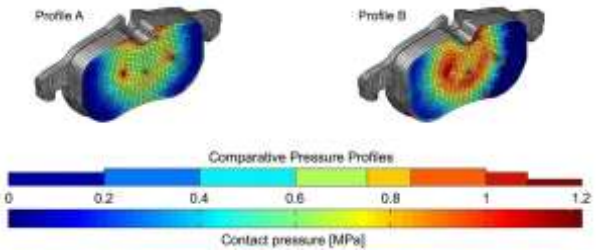


Fig. 8. Contact-pressure maps (MPa) showing the effect of tangential frictional traction on the pad.

2. Wear Evolution and Running-In

Over 2900 rotor revolutions (≈2500 m of sliding), wear progressively redistributes pressure over the pad face. Without friction traction, the pressure peak under the piston rim gradually flattens into a more uniform central contact zone (Fig. 9), and the corresponding wear profile is concentrated where the initial pressure was highest (Fig. 10). Under combined sliding friction, the initial leading-edge peak is reduced as the worn surface conforms to the rotor, and the pressure field stabilises into an equilibrated profile (Fig. 11). The wear-depth contours (Fig. 12) show maximum material loss in the region of initial high pressure, and the surface profile develops accordingly as wear accumulates. This smooth transition from localised peaks to steady-state pressure is the expected running-in behaviour.

International Journal of Science, Engineering and Technology
ISSN: 2348-4098, P-ISSN: 2395-4752

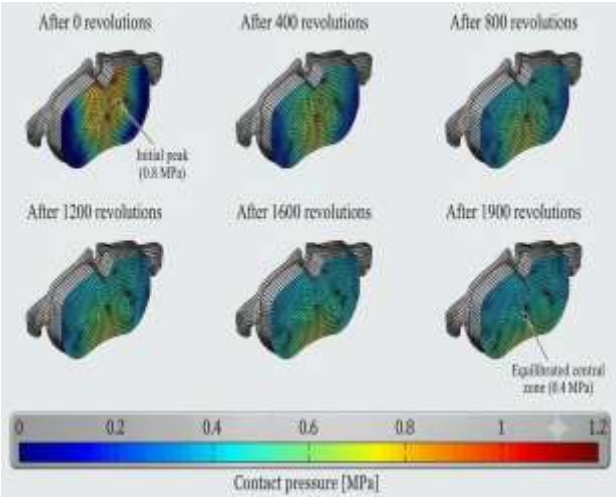


Fig. 9. Smoothing of contact pressure (MPa) with revolutions in the absence of tangential frictional traction.

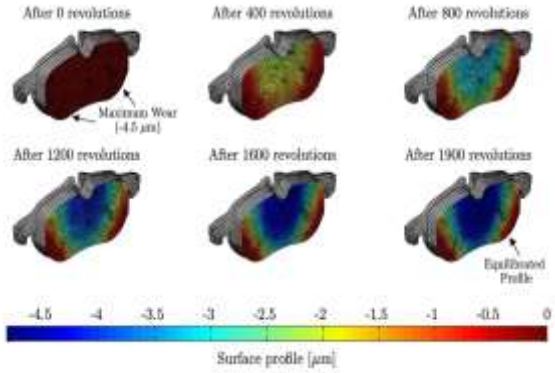


Fig. 10. Pad wear depth profile (μm) without tangential frictional traction.

The two loading cases differ in an important way. Without traction, the wear is axisymmetric about the piston and the pad wears into a central, nearly uniform contact zone. With traction, the initial pressure and wear are asymmetric, so the pad wears more at the leading side first, and the final equilibrated contact zone is displaced accordingly. This indicates that predictions of pad taper and uneven wear require the tangential load to be modelled, and that the running-in life depends on the loading case as well as on the material.

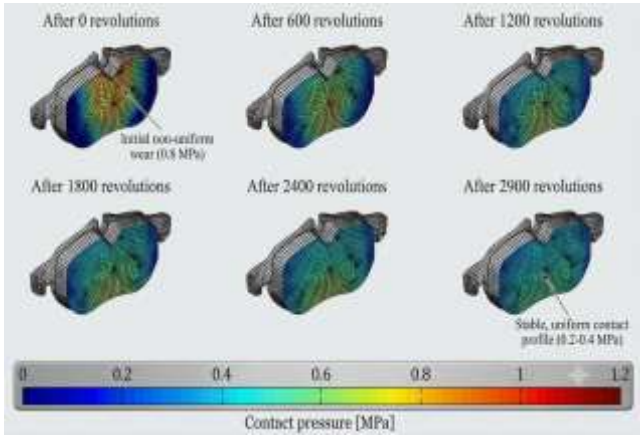


Fig. 11. Evolution of contact pressure (MPa) with rotor revolutions under combined sliding friction.

International Journal of Science, Engineering and Technology
ISSN: 2348-4098, P-ISSN: 2395-4752

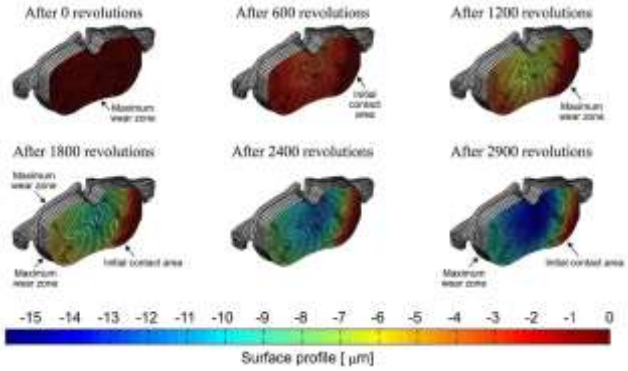


Fig. 12. Pad wear (surface profile, µm) at successive revolutions under combined sliding friction.

3. Comparison of Friction Materials

Table II summarises the three linings. The organic lining, with the lowest stiffness (10 GPa), conforms quickly and reaches steady-state pressure after 2400 revolutions, but wears most (15.0 µm). The semi-metallic lining gives a balance of stiffness and wear resistance (6.2 µm; 4100 revolutions). The ceramic-matrix composite wears least (2.1 µm), but its stiffness (35 GPa) produces the highest initial peak pressure (2.10 MPa) and the longest running-in (5800 revolutions).

Table Ii Simulated Pressure, Wear And Running-In

Material	Initial peak (MPa)	Steady state (MPa)	Max. wear (µm)	Running-in (rev.)
Organic composite	1.20	0.68	15.0	2400
Semi-metallic	1.65	0.74	6.2	4100
Ceramic-matrix	2.10	0.82	2.1	5800

A simple check using (3) supports the trend. Taking the steady-state pressure as constant over 2500 m gives h ≈ k p s of 17, 8.3 and 3.1 µm for the three linings. These upper-bound estimates are of the same order as, and slightly above, the simulated maxima, as expected because pressure is higher than the steady value only early in the run. The ranking of wear depth follows the ranking of k, while the ranking of peak pressure and running-in follows stiffness. Thus the lowest-wear material is not automatically the best choice: stiffer linings concentrate pressure and take longer to bed in, so the selection must balance wear life, running-in behaviour, friction level and thermal stability.

V. ADVANTAGES, LIMITATIONS AND APPLICATIONS

The approach reduces dependence on repeated dynamometer tests, captures friction-induced pad tipping that normal-load-only models miss, allows quick substitution of lining materials, and reveals running-in kinetics. Its limitations are the high computational cost of 3-D nonlinear contact with iterative wear loops; strong sensitivity to the empirical wear coefficient k, which varies with temperature, humidity and speed; the isothermal assumption, which neglects flash temperature and thermal-expansion mismatch [18]; and the rigid treatment of the piston, rotor and caliper, which may underestimate housing compliance. The method is applicable to passenger-car brake and pad-geometry design, electric-vehicle friction braking following regeneration, heavy-vehicle brakes and clutches, and high-performance ceramic-composite brake systems.

VI. CONCLUSION AND FUTURE SCOPE

A 3-D FE framework combining modular system modelling with an explicit-Euler Archard wear routine was used to study contact pressure and wear in a passenger-car brake pad. The main findings are:

International Journal of Science, Engineering and Technology
ISSN: 2348-4098, P-ISSN: 2395-4752

- Static loading of 2.5 kN produces a symmetric pressure peak of ≈1.2 MPa under the piston rim; adding friction (μ = 0.45) causes leading-edge concentration and trailing-edge separation.
- Iterative wear over 2900 revolutions (≈2500 m) smooths localised peaks into a steady-state pressure profile, reproducing running-in.
- Maximum wear falls from 15.0 μm (organic) to 6.2 μm (semi-metallic) and 2.1 μm (ceramic), but peak pressure rises from 1.20 to 2.10 MPa and running-in lengthens from 2400 to 5800 revolutions.

These results are model predictions based on assumed wear coefficients and are not experimentally validated. Future work includes: fully coupled thermo-mechanical analysis with temperature-dependent properties; squeal and NVH analysis using complex eigenvalue methods; wear coefficients that depend on temperature, pressure and velocity, k(T, p, v), calibrated by pin-on-disc tests; optimisation of pad slots and chamfers; flexible caliper modelling; and extension to regenerative braking duty cycles in electric vehicles.

REFERENCES

1. J. F. Archard, "Contact and rubbing of flat surfaces," J. Appl. Phys., vol. 24, no. 8, pp. 981–988, 1953.
2. A. Söderberg and S. Andersson, "Simulation of wear and contact pressure distribution at the pad-to-rotor interface in a disc brake using general purpose finite element analysis software," Wear, vol. 267, no. 12, pp. 2243–2251, 2009.
3. Ș. Voloacă, A. Badea-Romero, F. Badea-Romero, and M. F. Toma, "Motor vehicle brake pad wear—A review," Vehicles, vol. 7, no. 2, Art. no. 52, 2025.
4. Z. Tang, H. Yin, J. Zhao, and C. Ding, "Coupled wear-thermal-structural multiphysics field analysis of friction linings in disk brakes," Proc. Inst. Mech. Eng. D, J. Automob. Eng., vol. 239, no. 23, pp. 9765–9779, 2025.
5. G. S. Gurumoorthy, S. Grandhi, and S. S. Sridhar, "Brake pad wear prediction using finite element techniques," SAE Tech. Paper 2021-01-0810, 2021.
6. G. Riva, J. Wahlström, and A. Alemani, "An FEA approach to simulate disc brake wear and airborne particle emissions," Tribol. Int., vol. 138, pp. 90–98, 2019.
7. G. Riva, F. Varriale, and J. Wahlström, "A finite element analysis (FEA) approach to simulate the coefficient of friction of a brake system starting from material friction characterization," Friction, vol. 9, pp. 191–200, 2021.
8. Z. Sha, Q. Hao, J. Yin, F. Ma, Y. Liu, and S. Zhang, "Wear calculation and life prediction model of disc brake based on elastoplastic contact mechanics," Adv. Mech. Eng., 2022.
9. Z. Zhang et al., "Simulation study on friction and wear law of brake pad in high-power disc brake," Math. Probl. Eng., vol. 2019, Art. no. 6250694, 2019.
10. M. J. Han, C. H. Lee, T. W. Park, J. M. Park, and S. M. Son, "Coupled thermo-mechanical analysis and shape optimization for reducing uneven wear of brake pads," Int. J. Automot. Technol., vol. 18, pp. 1027–1035, 2017.
11. A. R. Abu Bakar and H. Ouyang, "Prediction of disc brake contact pressure distributions by finite element analysis," Jurnal Teknologi, vol. 43, no. 1, pp. 21–36, 2005.
12. H. Ouyang, A. R. Abu-Bakar, and L. Li, "A combined analysis of heat conduction, contact pressure and transient vibration of a disk brake," Int. J. Veh. Des., vol. 51, nos. 1–2, pp. 190–206, 2009.
13. N. A. Stoica, A.-M. Petrescu, and A. Tudor, "Modelling the wear processes of the automotive brake pad and disc," INCAS Bull., vol. 10, no. 4, pp. 169–179, 2018.
14. B.-C. Goo, "A study on the contact pressure and thermo-elastic behavior of a brake disc-pad by infrared images and finite element analysis," Appl. Sci., vol. 8, no. 9, Art. no. 1639, 2018.
15. P. Grześ et al., "Initial selection of disc brake pads material based on the temperature mode," Materials, vol. 13, no. 4, Art. no. 873, 2020.
16. A. Olshevskiy, A. Olshevskiy, O. Berdnikov, and C.-W. Kim, "Finite element analysis of railway disc brake considering structural, thermal, and wear phenomena," Proc. Inst. Mech. Eng. D, J. Automob. Eng., vol. 226, no. 7, 2012.

17. H.-J. Cho and C.-D. Cho, "A study of thermal and mechanical behaviour for the optimal design of automotive disc brakes," Proc. Inst. Mech. Eng. D, J. Automob. Eng., vol. 222, no. 6, pp. 895–915, 2008.
18. D. Li, D. Sun, H. Xi, and J. Dai, "Review on the mechanism of failure mode based on mechanical performance analysis of brake disc," Adv. Mech. Eng., vol. 16, no. 12, 2024.